Landslide-Bridge Interaction

A combined approach based on InSAR data and numerical modelling

Cernuto, Erica; Salciarini, Diana; Ubertini, Filippo; Giardina, Giorgia

DOI
10.1016/j.ijdrr.2025.105568

Publication date
2025

Document Version
Final published version

Published in
International Journal of Disaster Risk Reduction

Citation (APA)
Cernuto, E., Salciarini, D., Ubertini, F., & Giardina, G. (2025). Landslide-Bridge Interaction: A combined approach based on InSAR data and numerical modelling. *International Journal of Disaster Risk Reduction*, *126*, Article 105568. https://doi.org/10.1016/j.ijdrr.2025.105568

International Journal of Disaster Risk Reduction 126 (2025) 105568

Contents lists available at ScienceDirect

International Journal of Disaster Risk Reduction

journal homepage: www.elsevier.com/locate/ijdrr

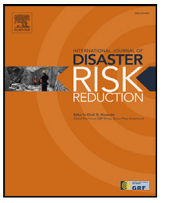

Landslide-Bridge Interaction: A combined approach based on InSAR data and numerical modelling

Erica Cernuto [a], Diana Salciarini [a], Filippo Ubertini [a], Giorgia Giardina [b,*]

[a] Department of Civil and Environmental Engineering, University of Perugia, Via Goffredo Duranti, 93, Perugia, 06126, Italy
[b] Department of Geoscience and Engineering, Delft University of Technology, Stevinweg 1, Delft, 2628 CN, The Netherlands

ARTICLE INFO

Keywords:
Remote sensing
Finite Element Modelling
Displacement monitoring
Landslide-infrastructure interaction

ABSTRACT

Landslides that interact with infrastructure, such as bridges, demand a comprehensive analysis to fully understand and address the complexities of this interaction. This study proposes an integrated approach that combines InSAR satellite monitoring with three-dimensional numerical modelling to analyse the effect of a landslide on a bridge. Although the case study is exemplary, the results obtained are of a general nature and applicable to similar contexts. The integration of InSAR and numerical modelling provided complementary and more detailed information compared to the isolated use of each approach. The InSAR analysis offered an overview of surface deformations, allowing for large-scale monitoring of movements, and its limitation in providing complete three-dimensional information was addressed by the numerical modelling, which enabled the decomposition of movements along the main direction of the landslide, precisely identifying the movement trajectory. The results showed predominant movements in the transverse direction, with a less significant vertical component, consistent with the observed kinematics. InSAR data allowed for the comparison of numerical modelling estimates with real observations, enhancing the consistency of the simulations. These data revealed significant movements upstream of the bridge, confirming the critical areas identified by modelling, which compensated for the lack of satellite data downstream, showing intense displacements. The modelling also highlighted significant displacements in the bridge's structural elements, with downstream tilting caused by the horizontal thrust of the landslide. The integrated approach offered a clearer understanding of landslide dynamics and their impact on infrastructure, offering a valuable tool for monitoring and risk management in vulnerable areas.

1. Introduction

Landslides represent an increasing global threat [1,2], with potentially devastating effects on critical infrastructure such as bridges and viaducts, which may suffer severe structural damage. In extreme cases, landslide movements can lead to displacements or rotations of substructures, resulting in deck collapse [3–5]. The risk associated with these events is amplified by their often-unpredictable nature, linked to the complexity of triggering factors and the possibility of occurring without warning signs. Recent studies [6,7] highlight the challenges in correlating landslide types with structural damage due to the variability of landslides in terms of volume, kinematics, material composition, and orientation. Furthermore, landslide movements can impact bridges in longitudinal [8] and transverse directions [9], with either partial or total interference.

* Corresponding author.
E-mail address: g.giardina@tudelft.nl (G. Giardina).

https://doi.org/10.1016/j.ijdrr.2025.105568
Received 20 December 2024; Received in revised form 16 April 2025; Accepted 9 May 2025
Available online 29 May 2025

Despite numerous studies on real-world cases of bridge-landslide interactions, models capable of accurately simulating structural responses to different types of interaction do not yet exist. For a reliable assessment of infrastructure safety in landslide-prone areas, a possible approach could be the integration of data acquired through modern ground surface movement monitoring technologies with robust numerical models. In this context, Synthetic Aperture Radar Interferometry (InSAR) has emerged as one of the most promising technologies for large-scale landslide monitoring [10,11]. InSAR is particularly effective for detecting small deformations of the Earth's surface over extended periods, without the need for ground-based instrumentation and offering relatively low costs, making it suitable for monitoring areas that are challenging to access with conventional methods.

Among the most commonly used interferometric techniques for landslide analysis, PS-InSAR allows for the reconstruction of displacement time series and the detection of ongoing or past deformation processes [12]. In particular, it has proven effective in studying slow-moving landslides, enabling the assessment of their activity state and intensity [13,14].

In SAR remote sensing systems, the radar detects ground-based targets by measuring the distance between the sensor and the target along the Line of Sight (LOS), which is the line connecting the sensor to the target, inclined at an angle θ (off-nadir) relative to the vertical [15,16]. The detected displacements are thus one-dimensional projections of movements along the LOS, a significant limitation since deformations occur in a three-dimensional space and the radar only measures the component along the LOS. Consequently, displacements may be underestimated or not detected if the deformation occurs perpendicular to the LOS [17].

The above described limitation is particularly critical for landslides, which often exhibit horizontal deformation components that are almost not detectable along the LOS of the satellite [18,19]. To address this limitation, LOS data must be transformed into three-dimensional displacement components. This process involves post-processing operations that rely on specific assumptions about the moving object's trajectory, inevitably introducing a bias error. In this context, numerous approaches have been proposed in the literature to convert LOS displacements into true three-dimensional components [20–24]. However, a uniform and standardised method to effectively tackle this challenge has not yet been established.

Moreover, for an accurate estimation of the actual displacement components, it is essential that the available LOS measurements are spatially and temporally independent and coincident. In other words, the ascending and descending acquisitions must refer to the same "Persistent Scatterers" in the study area and occur simultaneously. Since these conditions are rarely met, further post-processing operations, such as resampling and temporal alignment, are required. Among the approaches developed to combine ascending and descending datasets, authors in Manzo et al. [25] propose a raster-based method that uses common pixels in the velocity maps from both geometries, while authors in Casagli et al. [26] and Proietti [22] suggest a vector-based resampling on a regular grid. Both methods combine LOS measurements to calculate vertical and horizontal displacement components on what are referred to as "synthetic PS". Another approach, proposed by Notti et al. [20], matches pairs of PS based on the geometric distance between points in the two orbital geometries. Despite the various methods proposed, it is not possible to identify the most effective one for application in landslide-prone areas, where factors such as vegetation influence the behaviour of the PS, making it challenging to apply solutions in a standardised way.

Despite continuous technological advances, InSAR alone presents certain inherent limitations in landslide monitoring—just as every monitoring technique has its own drawbacks. In particular, while InSAR is essential for detecting surface deformations associated with landslides, it does not provide a complete understanding of landslide processes. In particular, InSAR is unable to detect movements occurring at greater depths, such as those along the sliding surface, nor to simulate the internal evolution of the landslide, aspects that can be more accurately analysed through numerical modelling. Therefore, to obtain a deeper understanding of these phenomena, it is useful to complement InSAR with numerical models capable of simulating landslide evolution and failure mechanisms, thereby enabling the prediction of future deformations, as demonstrated in recent literature. Styles et al. [27] used InSAR to calibrate numerical models for understanding deformations in open-pit mines. Ma et al. [28] employed InSAR data to determine soil properties through back-analysis, simulating complex landslide movements. Sun et al. [29] combined MSBAS-InSAR and numerical modelling to study landslides controlled by rock layers, improving efficiency and accuracy. Meoni et al. [30] integrated InSAR-based monitoring with visual inspections, geometric surveys, destructive and non-destructive tests, and numerical analyses, to diagnose and monitor slow deformations in bridges.

Understanding the processes governing landslide dynamics through both static and dynamic numerical simulations is relevant for effective risk management, particularly for infrastructure impacted by landslide movements. Although many studies have focused on two-dimensional approaches to analyse slope stability, which have significantly contributed to the development of numerical analyses, it is important to consider that in most cases landslides constitute typically three-dimensional problems [31]. In fact, 2D approaches may not fully account for the structural and morphological variations along the slip surface, potentially affecting the accuracy of the analysis. In contrast, three-dimensional (3D) numerical models provide a more detailed and accurate representation of landslide phenomena [32,33]. These models do not only enable the simulation of deformation evolution but also determine the direction of movement and the maximum velocity of the landslide [34,35]. Furthermore, they enable the reconstruction of the landslide trajectory, providing crucial information for identifying high-risk areas and analysing slope stability [36–39], thereby enhancing the understanding of landslide behaviour. 3D modelling is particularly effective in assessing interactions between landslides and infrastructure [40,41], as it allows for the simulation of deformation propagation along complex surfaces in both homogeneous and heterogeneous materials.

Among the numerical methods frequently employed for modelling such phenomena [42–44], the Finite Element Method (FEM) enables an accurate representation of deformation evolution under both static and dynamic conditions [45]. In this context, the choice of the constitutive model is a critical aspect of numerical modelling, as it allows for a realistic description of the mechanical properties of the soil, particularly for capturing its non-linear behaviour. Calibration of these models, however, requires precise input data, which are often limited or rely on direct investigations such as boreholes, inclinometers, extensometers, and piezometers,

providing only localised and point-specific information [46]. In some cases, indirect methods such as geophysical surveys can also contribute to the preliminary estimation of geotechnical parameters, particularly in areas where direct investigations are difficult to perform [47]. In this context, integration with InSAR offers a significant advantage by enabling large-scale monitoring and supplying valuable data for the calibration and/or validation of numerical models. In addition, InSAR observations can complement conventional monitoring, as the combined use of satellite data and ground-based instruments improves the geological interpretation of landslides and the understanding of their geometry and kinematics [48]. Thus, the combination of satellite data and numerical models presents a promising solution to achieve more accurate and reliable predictions.

This study aim to investigate the potentiality of a combined approach using InSAR satellite data and numerical modelling to analyse a landslide mechanism that partially interferes with a bridge, specifically with one of its abutments and some of its pier foundations. For this purpose, a numerical model was developed, supported by on-site monitoring, to characterise the landslide phenomenon and provide reliable predictions. For the InSAR data, a procedure was adopted to derive two-dimensional displacement components by projecting measurements from both ascending and descending orbits onto the assumed deformation plane. This process includes resampling, selected based on a comparative study of available approaches, and time alignment, both crucial for accurately estimating displacement components in a two-dimensional system. By integrating numerical modelling with InSAR data, the interaction between the landslide and the bridge can be simulated, identifying areas of increased vulnerability and stresses on the structure. This integrated approach offers a deeper understanding of landslide dynamics and their potential impact on infrastructure stability, making it a valuable tool for risk monitoring, mitigation, and ensuring safer management of infrastructure in landslide-prone regions. The work is structured as follows. Section 2 presents the case study, introduced to facilitate the understanding of the method, which is illustrated with reference to a practical example. Section 3 defines the proposed method, describing the combined approach that integrates InSAR data analysis with numerical modelling and details the procedures used. Section 4 presents the results of the analyses conducted. Section 5 presents a detailed discussion of the analyses, while Section 6 summarises the main conclusions and findings of this study. Note that the data used, solely for the purposes of this study, refer to past investigation campaigns and do not necessarily reflect current conditions. Any changes, modifications to the slope, or interventions installed on the bridge have not been considered in the model. It is clarified that this study does not aim to investigate the current stability conditions of the system or the landslide phenomenon. The case study is used exclusively to demonstrate the applicability of the approach.

2. Case study

The study area is located in a small municipality in the province of Parma, within the Emilia-Romagna region of Italy. It is characterised by complex geology and slopes with moderate inclinations ranging between 10° and 15°. This region exhibits significant geomorphological instability, typical of the northern Apennines, with numerous landslide phenomena, as highlighted in Fig. 1, derived from the "Italian Landslide Inventory" (IFFI) [49].

Among these, particular attention is drawn to a landslide identified as a roto-translational slide, which directly interferes with a motorway bridge. From a geological perspective, the area is characterised by the overthrust of the Scabiazza Sandstones (SCB and SCBb), located upstream of the motorway alignment, onto the Blocky Clays of the Casanova Complex (CCVb), which outcrop downstream. Interposed between these two formations there are lithologies of the Palombini Shale Formation (APA) (Fig. 2). This stratigraphy results in a configuration with sandstones in the upper portion and clays outcropping in the lower part of the slope, contributing to the area's geomorphological instability. Fig. 2 shows an extract from the geological map, derived from the Geological Mapping of the Emilia-Romagna Region [50], along with a geological cross-section of the site, which was elaborated by the authors based on confidential data.

The landslide develops upstream of the motorway alignment, impacting the slope and causing progressive deformations and significant translational displacements. The progression of the phenomenon is evident on the road surface, which frequently exhibits cracks and fractures, requiring regular repair interventions. These movements have considerably impaired the functionality of the infrastructure, demanding continuous monitoring and consistent maintenance to ensure traffic safety and uninterrupted operation. Geotechnical surveys and instrumental monitoring conducted over time have enabled the characterisation of the landslide phenomenon and an understanding of its dynamics through geognostic surveys, grain size analyses, inclinometers, piezometers, and topographic targets (Fig. 3a).

Inclinometers (Inc1, Inc2, Inc3, Inc4, Inc5) were installed in the upstream portion of the landslide, near the road in the downstream section, and in the accumulation area. These instruments identified a sliding surface approximately 80 m deep (corresponding to inclinometer Inc5, (Fig. 3b)) and an average landslide movement of 6.5 cm per year. However, due to intense ground deformations, such measurement devices are no longer functional. To complement the inclinometer monitoring, topographic targets (Fig. 3a) were installed to track the surface movements of the landslide. The topographic monitoring initially involved the installation of 14 targets in 1975, with 13 placed near the highway roadway and one positioned at the corner head of a building. This monitoring continued until 1999, during which 12 readings were conducted, recording an average displacement velocity consistent with inclinometric data, converging to a value of 6.5 cm/year (Fig. 3d). In subsequent years (2004–2015), additional benchmarks were installed along the carriageways and in the areas affected by the landslide. The collected data indicated higher displacement rates upstream of the motorway (exceeding 6 cm/year), while targets positioned downstream of the motorway recorded average annual velocity above 5 cm/year (Fig. 3d). To better understand the landslide movements, new inclinometers (G1, G2, G3) were installed in 2015, providing updated data (Fig. 3a). These instruments detected displacements of 4–6 mm per month at a depth of approximately 37–38 m, along the G1 and G3 verticals, further confirming the active nature of the landslide.

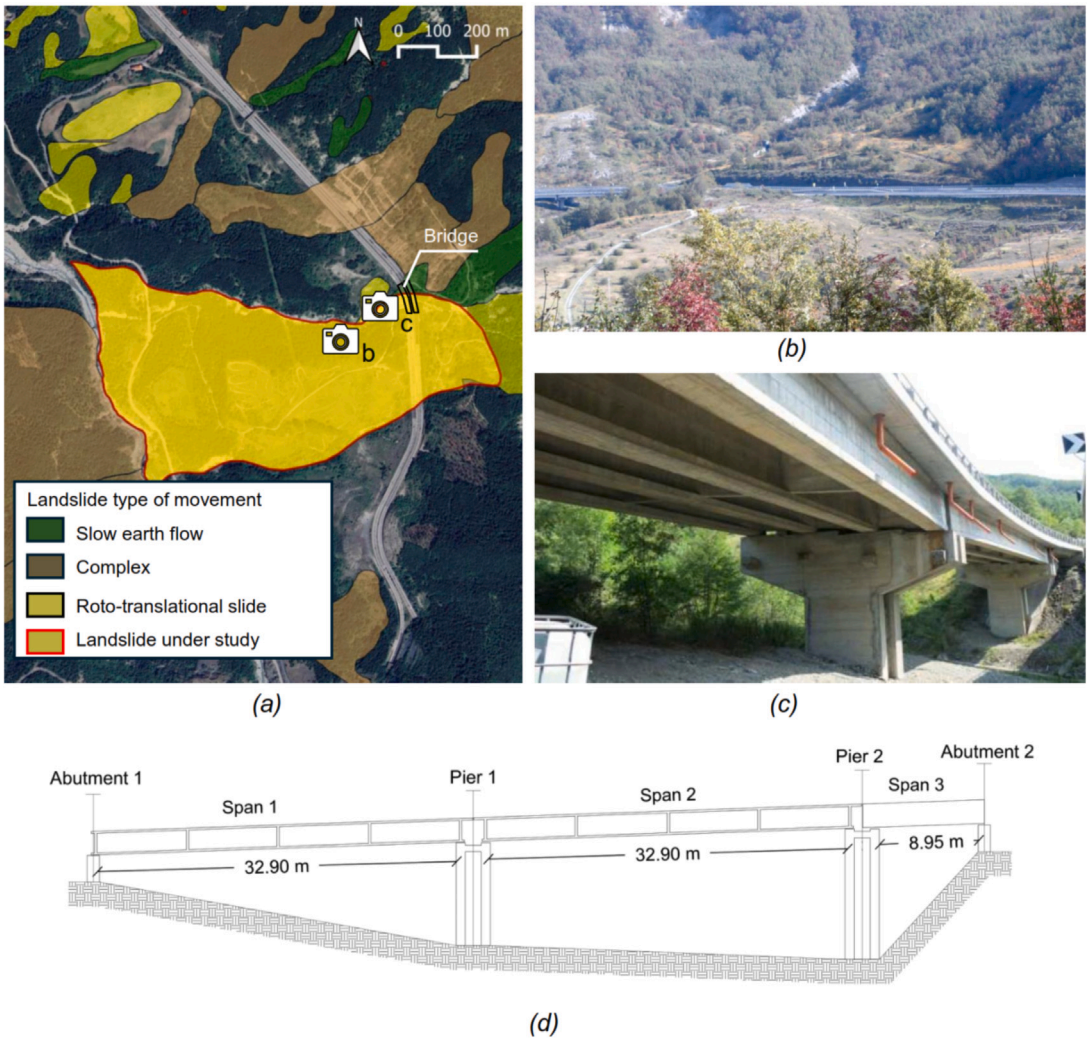

Fig. 1. (a) Extract from the cartography of the Italian Landslide Inventory (IFFI), highlighting the landslide under investigation; (b) Panoramic view of the area affected by the landslide, near the bridge; (c) View of the bridge; (d) Reconstruction of schematic longitudinal section of the bridge.

Moreover, grain size analyses conducted on six samples, collected from boreholes SG3 and SG5, selected as the most significant due to their central location for the characterisation of the landslide, revealed that the landslide material is characterised by a fine silty-clayey matrix. Therefore, the main predisposing factors for instability include the composition of the material and the presence of water in the soil. This creates a free water table with a piezometric surface close to the ground level, further worsening the stability of the slope. The landslide geometry is defined by a length of 1000 m, an average width of 300 m, an average slope inclination of 10°, and a maximum depth of the sliding surface, identified through inclinometric surveys, of 80 m. Piezometric data from six borehole-installed piezometers confirm the presence of a water table located very close to the ground surface, significantly heightening the risk of instability.

The bridge, which interferes with the landslide, consists of three spans (Fig. 1c): the first two, each with a span length of 32.9 m, feature a grid deck composed of four simply supported post-tensioned precast concrete beams, while the third span, with a length of 8.95 m, consists of a reinforced concrete slab (Fig. 1d). The structure is supported by two piers and the retaining walls of the abutments, both made of reinforced concrete. The foundations of the piers and abutments consist of large diameter caissons: approximately 6 m for the abutments and 7 m for the piers. Each caisson is encased in a 50-*cm*-thick concrete lining and extends to a depth of approximately 12 m.

3. Methodology

The methodological approach proposed in this study integrates InSAR satellite monitoring with numerical modelling to analyse the interaction between the landslide and the bridge. Combining these techniques provides insights that would not be accessible

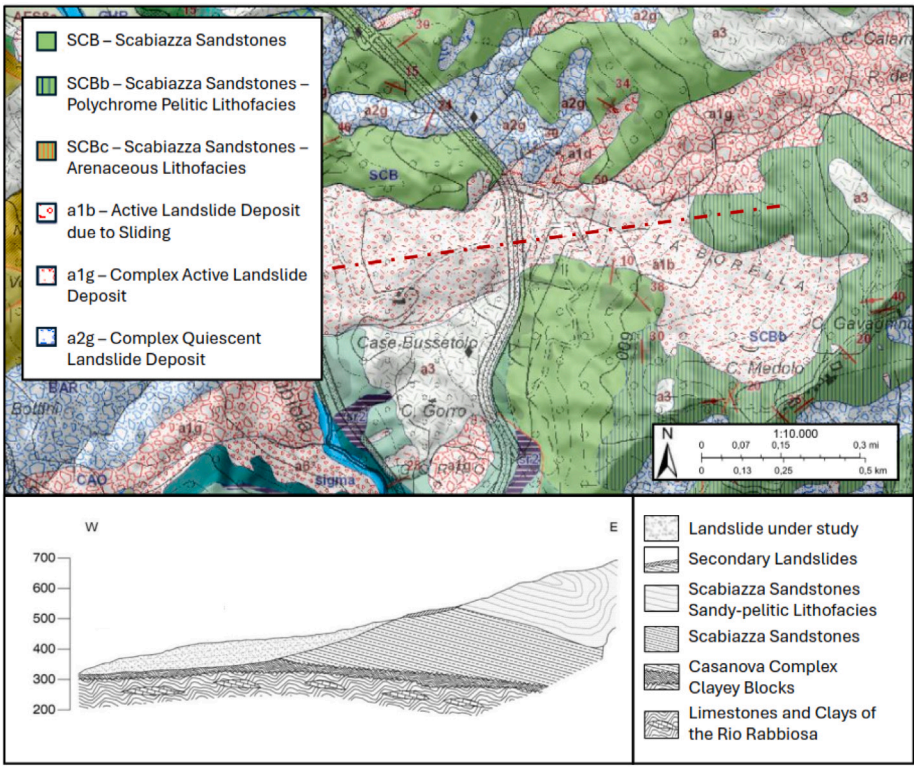

Fig. 2. Extract from the Geological Mapping of the Emilia-Romagna Region (scale: 1:10.000) and Geological cross-section along the landslide.

using a single method, making this integration a key element for achieving a more comprehensive understanding of the phenomenon. InSAR analyses enable large-scale monitoring of surface deformations and the time evolution of displacements during the observation period. However, converting movements along the Line of Sight (LOS) into accurate three-dimensional components is inherently ill-conditioned, necessitating supplementary information to achieve reliable estimates. In this context, numerical modelling is employed to simulate the three-dimensional behaviour of the landslide and to define the primary direction of movement, determined by the slope topography and following the trajectory of maximum slope, which corresponds to the line perpendicular to the contour lines. Furthermore, while numerical modelling provides a detailed representation of the landslide behaviour and movement direction, it does not independently offer a direct reference to determine if the obtained displacements are consistent with the actual behaviour of the phenomenon. In the absence of direct observations, verifying that simulations accurately represent the dynamics of the landslide becomes challenging. Conversely, satellite data provide direct information on surface movements, which can be used to compare numerical modelling estimates with real-world observations. As highlighted in the flow chart shown in Fig. 4, the methodological process includes an initial phase of data acquisition and processing, followed by a parallel analysis through numerical modelling and InSAR data analysis. The obtained results are then combined to provide a more coherent and detailed understanding of the landslide evolution. This iterative process ensures that each method helps address the limitations of the other, enhancing both the reliability of numerical simulations and the interpretation of InSAR data.

3.1. Numerical modelling

The numerical modelling was performed using the finite element software Plaxis 3D [51], a three-dimensional programme widely employed in geotechnical applications, including the analysis of the soil–structure interaction problem [52–55]. The topography of the soil was defined using contour lines with a 5 *m* interval, produced in 2021 [56], to accurately represent the actual morphology of the site (Fig. 5). The soil was modelled as a homogeneous and non-stratified volume, composed of a silty-clayey material, determined based on grain size analyses. The landslide under study was reproduced in the model, with its dimensions provided in Section 2, and is characterised by a roto-translational movement along a sliding surface (Fig. 5).

The model considered two main volumes: stable soil and landslide (Fig. 5). The materials associated with these two portions have the same physical and mechanical properties, except for the mechanical strength parameters (cohesion and friction angle), which were calibrated through a back analysis using an iterative approach (Table 1). To represent the sliding surface between the two volumes (landslide and stable soil), a specific interface was defined (Fig. 5). The mechanical strength parameters associated with the interface were set in residual conditions, with significantly reduced values to simulate the sliding of the landslide along the failure

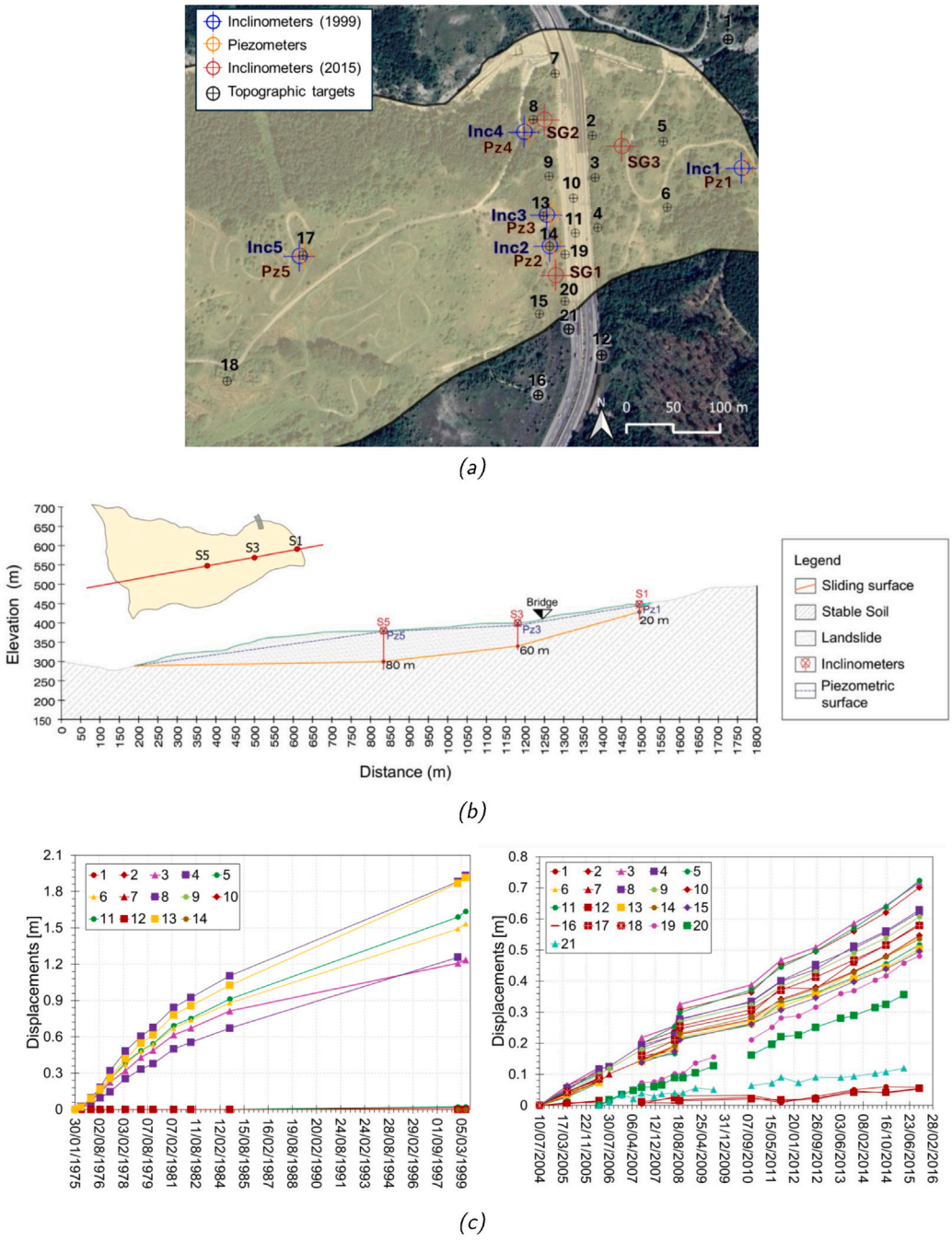

Fig. 3. (a) Plan showing the location of the instrumental monitoring conducted over the years; (b) Longitudinal section of the landslide area indicating the sliding surface depth, piezometric surface, and locations of inclinometers and piezometers; (c) displacements recorded during the monitoring period from topographic targets.

surface (Table 1). They were initially selected based on the geotechnical literature [57] and subsequently refined by means of a parametric study to suit the specific conditions of the site. This process ensured an accurate representation of the observed landslide behaviour, combining experimental results with numerical calibration to obtain parameters consistent with the phenomenon under study.

The Hardening Soil (HS) constitutive model [58,59] was assigned to all materials to simulate their non-linear behaviour, and particularly their variation in stiffness as a function of strain level. The model can simulate both soft and stiff soils, with a distinct capability to capture the behaviours of shear and compression hardening.

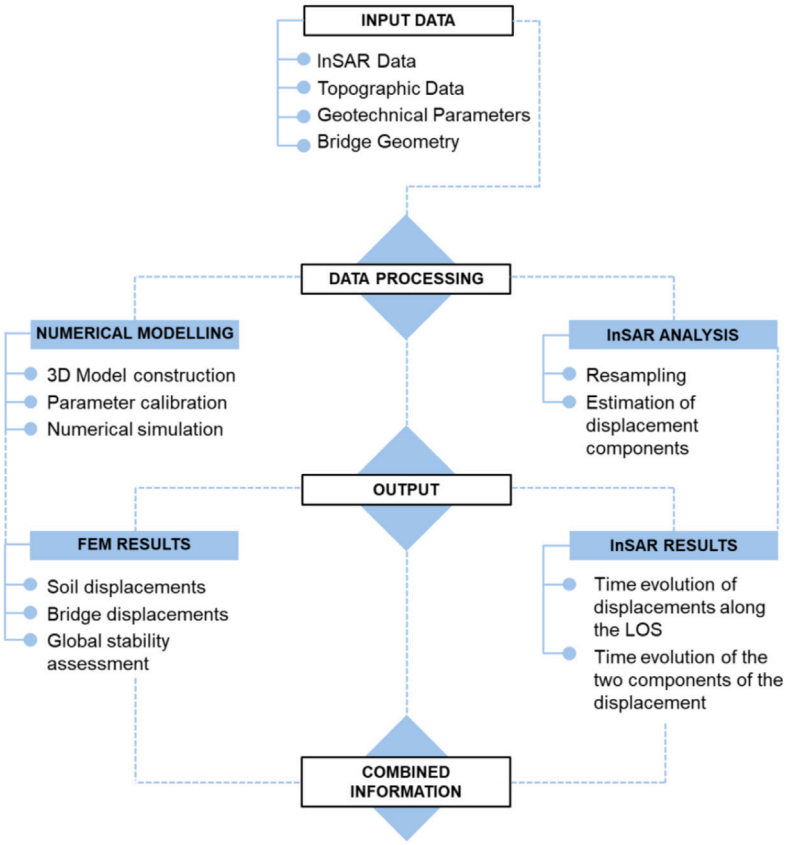

Fig. 4. Flowchart of the adopted methodology.

Table 1
Strength parameters adopted for stable soil, landslide volume and sliding surface.

Parameter	Soil volume	Landslide volume	Sliding surface	Unit
Cohesion (c')	30	28	1	kN/m^2
Friction angle (φ')	35	30	18	°
Dilatancy angle (ψ)	2	2	0	°

In the HS model, soil stiffness is characterised by three distinct parameters, which were defined based on the geotechnical properties of the soil in the study area and the available literature. The first is the secant stiffness modulus (E_{50}^{ref}), defined in accordance with the ranges reported by Schanz et al. [60] (Table 2). The other two parameters, the unloading/reloading modulus (E_{ur}^{ref}) and the oedometer modulus (E_{oed}^{ref}), were determined using commonly adopted empirical relationships [61]. The oedometer modulus reflects the soil behaviour under one-dimensional compression, while the unloading/reloading modulus represents the higher elastic stiffness observed during unloading and reloading cycles, in line with the values suggested by Schanz et al. [60] (Table 2). Furthermore, the model includes the parameter m, which describes the dependency of soil stiffness on effective stress, enhancing the representation of soil behaviour under variable loading conditions (Table 2). It also allows for the yield surface to evolve within the principal stress space in response to plastic deformations, further refining the accuracy of the soil behaviour representation [61]. The parameter m was adopted in accordance with the values suggested by Janbu [62] and Wu and Tung [63], making it particularly suitable for soils such as sands and silts. Shear strength parameters, such as cohesion c, friction angle (ϕ), and dilation angle (ψ), are used to describe the lateral deformations of the material during sliding.

After defining the soil geometry and its characteristics, the structural elements of the bridge were modelled, with the geometric characteristics provided in Section 2, taking into account the partial interference with the analysed landslide phenomenon (Fig. 5d). Simplifications were applied to the elevated structures, as the primary focus was on geotechnical aspects and the interaction between the soil and the foundations. In particular, the piers were modelled as beams with linear elastic behaviour, while the deck was represented as a beam with a simply supported static configuration. The final mesh of the model consists of 13362 tetrahedral 10-nodes elements (Fig. 5d), ensuring a detailed representation of the soil geometry.

Lastly, the presence of water in the soil was considered, resulting in a free water table close to ground level. To represent this condition, the piezometric surface was incorporated into the model at 2.5 m below ground level. The model analysis develops

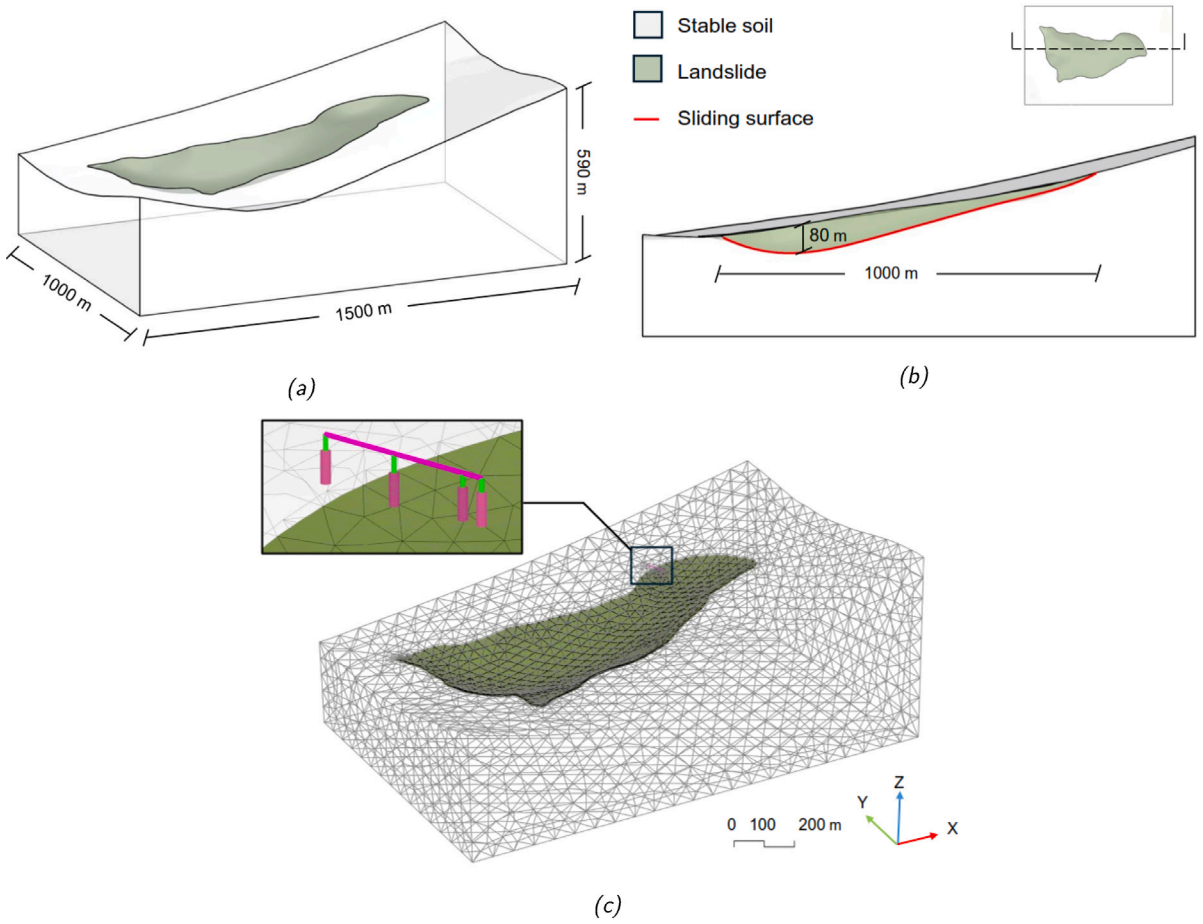

Fig. 5. (a) 3D view of the three-dimensional soil model; (b) Longitudinal cross-section of the three-dimensional soil model; (c) Three-dimensional view of the model with the bridge integrated in Plaxis 3D.

Table 2
Hardening soil constitutive model parameters assigned for model materials.

Parameter	Value	Unit
Secant stiffness (E_{50}^{ref})	30.00×10^3	kN/m^2
Tangent stiffness (E_{oed}^{ref})	36.01×10^3	kN/m^2
Unloading/reloading stiffness (E_{ur}^{ref})	110.80×10^3	kN/m^2
Power for stiffness dependency on stress level (m)	0.5	–

through progressive phases, starting with the definition of the initial stress state of the soil and continuing with the plastic phase to study the elastoplastic deformation. Finally, a global stability analysis, based on the strength reduction method, allows for the assessment of the overall stability and the response of the model.

3.2. Satellite data analysis

The satellite data analysis for the study area was carried out using InSAR data derived from and processed by Sentinel-1, accessed through the European Ground Motion Service (EGMS) of the Copernicus program, managed by the European Environment Agency [64] (Fig. 6). This publicly available and free service provides point measurements of ground displacement (Permanent Scatterers, PS) with a temporal resolution of six days [65]. Each PS is associated with an annual average deformation velocity (in mm/year) measured along the line of sight of the sensor. This value, recorded over the acquisition period, determines the colour of each point according to a colour scale. By convention, a traffic light scheme centred at zero is used: stable points (with velocities between ±1.5mm/year) appear in green, those with positive velocities (movement toward the satellite) are shown in gradations from light blue to blue, and those with negative velocities (movement away from the satellite) are displayed in gradations from yellow to red. Additionally, EGMS offers three levels of products updated annually: Basic, Calibrated, and Ortho. Although the Ortho product

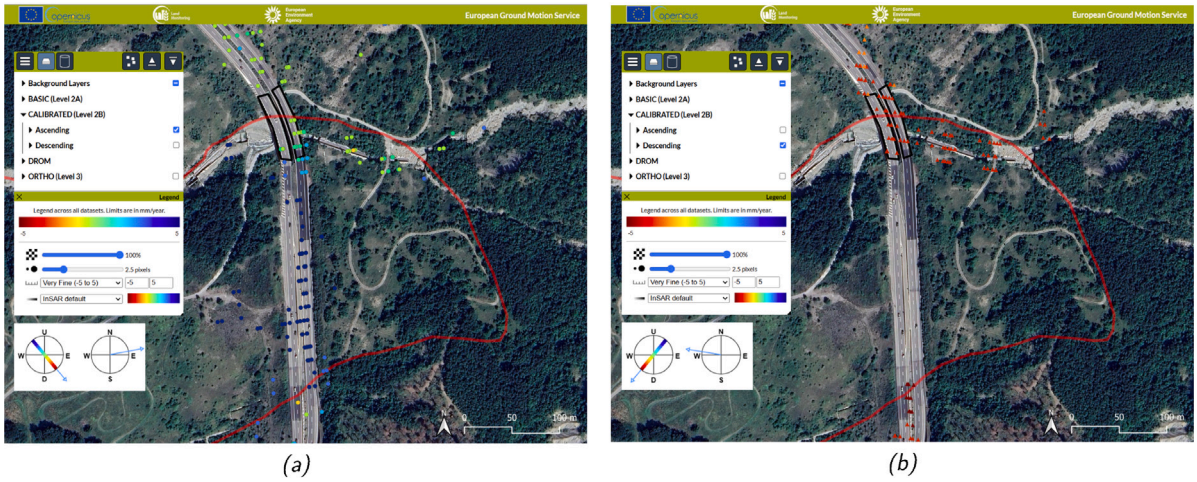

Fig. 6. Identification of the area of interest in the European Ground Motion Service (EGMS) of the Copernicus program: (a) Ascending dataset; (b) Descending dataset.

(Level 3) directly provides the horizontal and vertical displacement components, these are obtained through resampling onto a 100 m grid, significantly reducing the number of available points within the area of interest. In this specific case, the Ortho product identifies only two points, which greatly limits the analysis of the landslide kinematics and its interaction with the infrastructure. Beyond the loss of spatial resolution, another limitation concerns the reference system used in the Ortho product, which expresses displacement components in the ETRS89-LAEA system, with East, North, and Vertical directions. While this system is widely used, it is not always optimal for representing actual displacement, as it is not aligned with the orientation of the deformation phenomenon. To overcome these limitations, this study chose to use the Calibrated (Level 2B) product which, unlike the Basic (Level 2 A) product, combines and calibrates the InSAR measurements, obtained along the satellite's line of sight, with a reference model derived from GNSS (Global Navigation Satellite System) data. This makes it possible to obtain displacements referenced to a terrestrial reference system, rather than relative to a virtual reference point, and is available in ascending and descending geometry. Furthermore, to ensure a more coherent representation of the actual movement, a local reference system (L, T, V) was adopted, fixed to the deformation phenomenon, providing a more consistent interpretation of the real displacement.

In this study, datasets related to ascending (06/01/2018–23/12/2022) and descending (05/01/2018–22/12/2022) orbital geometries were analysed, ensuring consistent temporal and spatial coverage for the study area. For the purpose of satellite data analysis, the intrinsic limitation of these techniques, linked to the nature of the measurements, was taken into account. Interferometric techniques allow for the detection of deformation and velocity components exclusively along the Line of Sight (LOS), which corresponds to the vector connecting the sensor and the target. Consequently, PS data provide information limited to the LOS component of the actual displacement vector. This means that when real movements do not occur parallel to the LOS - as is often the case in landslides with significant horizontal components - the measured velocity and displacement values may be underestimated relative to the actual ones. To address this limitation and accurately reconstruct the real displacement components, post-processing of the data is required. Specifically, it is crucial to ensure that ascending and descending acquisitions are independent and both spatially and temporally consistent before converting LOS measurements into real components. This requires that the PS observed by the two geometries correspond in both space and time, with the same PS being simultaneously observed in both geometries. Since these conditions are rarely satisfied, spatial and temporal interpolation techniques must be applied to align and make the datasets consistent. Based on this, the proposed methodology is organised into two main phases:

- *Resampling Method*. The resampling process was carried out using a regular grid with square meshes measuring 25 m per side (Fig. 7a), designed based on the density of PS in the ascending and descending geometries. This mesh size was chosen to ensure a sufficient number of PS within each mesh element, considering the heterogeneous distribution of the data. Specifically, in the landslide area, where vegetation is predominant, the PS density is lower compared to that observed around the bridge. Due to the limited availability of dual-orbital geometry data downstream of the landslide, the analysis focused on the upstream section, where interaction with the infrastructure occurs. The grid configuration was selected following a comparative analysis of different approaches. One method, proposed by Notti et al. [20], involves pairing PS from the two geometries using linear interpolations and a 7 m buffer to identify synthetic points. Another approach, based on the method of [26], employs a regular mesh with 50 m sides. However, both methods revealed significant limitations, primarily due to outliers in displacement values caused by the presence of vegetation, whose signal is influenced by wind and seasonal variations, as discussed in more detail in the following sections. Therefore, adopting a smaller mesh grid allowed us to overcome these limitations. Once the grid size was defined, at the centroid of each mesh element, a synthetic PS was defined for each orbital geometry (Fig. 7b and c), calculated as the average of the LOS displacement values of the PS contained within the mesh across all acquisition dates. This approach

enabled the derivation of a single temporal evolution representing the average behaviour of the PS within each mesh element. Since ascending and descending acquisitions do not occur simultaneously, post-processing operations were applied to align the two datasets and ensure their consistency. Specifically, considering only the common time interval (06/01/2018–22/12/2022) between the two datasets, an interpolation of the time series was performed to estimate the missing displacement values corresponding to acquisition dates present in one geometry but absent in the other. Subsequently, the synthetic PS defined for each geometry were combined, excluding those present in one geometry but not in the other (Fig. 7d). This process produced a single consistent temporal dataset for each synthetic PS, containing the LOS displacement values for both geometries.

- *Estimation of the Actual Displacement Components*. The proposed method for estimating the actual displacement components is based on an adaptation and combination of the approaches presented by Brouwer [21] and Farneti et al. [23], suitably modified for the case under study. The estimation of the actual displacement (d) is determined based on the deformation measured along the line of sight of the satellite (d_{LOS}) within a global reference system (E, N, V) (Fig. 8a), using the following equation:

$$d = \frac{d_{LOS}}{\mathbf{u}_d \cdot \mathbf{u}_{LOS}} = \frac{d_{LOS}}{\cos\theta\cos\omega + \sin\theta\sin\omega\cos(\alpha+\varphi)} \tag{1}$$

where the unit vectors u_d and u_{los} define the directions of the real displacement vector d and the d_{los} vector, respectively, with respect to the global reference system (E, N, V). Here, θ is the incidence angle between the Line of Sight (LOS) of the sensor and the Vertical axis (V); α is the angle between the projection of d_{LOS} onto the Horizontal plane (E, N) and the East axis (E); ω and ϕ are the vertical and horizontal angles that define the direction of the real displacement vector (d) in three-dimensional space. Although the global reference system is widely used, it is not always the optimal choice for accurately describing real displacement. Its global components (East, North, Vertical) may not align with the principal directions of displacement, which can occur in all three dimensions. To achieve a more accurate and meaningful representation of real displacement, a local reference system (L, T, V) fixed to the deformation phenomenon was adopted (Fig. 8b). In this system, the transverse direction (T) is defined to coincide with the principal direction of the real displacement of the landslide, determined through numerical modelling, in the horizontal plane.

Assuming that the actual displacement occurs exclusively along one of the three local directions (L, T, V) and that no other movement contributes to the LOS measurement at a given time, Eq. (1) becomes:

$$d_L = \frac{d_{LOS}}{\mathbf{u}_{dL} \cdot \mathbf{u}_{LOS}} = \frac{d_{LOS}}{\sin\theta\sin(\alpha+\varphi)} \tag{2}$$

$$d_T = \frac{d_{LOS}}{\mathbf{u}_{dT} \cdot \mathbf{u}_{LOS}} = \frac{d_{LOS}}{\sin\theta\cos(\alpha+\varphi)} \tag{3}$$

$$d_V = \frac{d_{LOS}}{\mathbf{u}_{dV} \cdot \mathbf{u}_{LOS}} = \frac{d_{LOS}}{\cos\theta} \tag{4}$$

The value measured along the Line of Sight (d_{LOS}) of the sensor can therefore be expressed as a linear combination of the real displacement components along the three directions of interest (d_L, d_T, d_V):

$$d_{LOS} = d_L \sin\theta\sin(\alpha+\varphi) + d_T \sin\theta\cos(\alpha+\varphi) + d_V\cos\theta \tag{5}$$

Where, u_{dl}, u_{dt}, and u_{dv}, represent the unit vectors corresponding to the three directions (L, T, V). In general, to estimate the complete three-dimensional displacement vector (d_L, d_T, d_V), acquisitions from at least three different Lines of Sight (LOS), not lying on the same plane, and coinciding in both space and time, would be required [66]. However, with only two orbital geometries (ascending and descending) available, the combination of the LOS measurements (d_A and d_D) with the real displacement components (d_L, d_T, d_V) leads to an underdetermined linear system, expressed as:

$$\mathbf{d}_{LOS} = \mathbf{A}\mathbf{d} \tag{6}$$

where:

$$\mathbf{d}_{LOS} = \begin{Bmatrix} d_A \\ d_D \end{Bmatrix},$$

$$\mathbf{A} = \begin{bmatrix} \sin\theta_A\sin(\alpha_A+\varphi) & \sin\theta_A\cos(\alpha_A+\varphi) & \cos\theta_A \\ \sin\theta_D\sin(\alpha_D+\varphi) & \sin\theta_D\sin(\alpha_D+\varphi) & \cos\theta_D \end{bmatrix},$$

$$\mathbf{d} = \begin{Bmatrix} d_L \\ d_T \\ d_V \end{Bmatrix}$$

To solve the system, it is necessary to introduce an additional assumption. In the case of landslide phenomena, where the primary movement occurs downslope with gravity as the driving force, it is reasonable to assume that there are no displacements in the longitudinal direction (d_L=0) [21]. This assumption is valid when the longitudinal direction is parallel to the contour lines of the slope, as in the case of purely gravity-driven landslides. Under these conditions, the presence of a longitudinal displacement component is unlikely, as the primary deformation follows the direction of maximum slope, which,

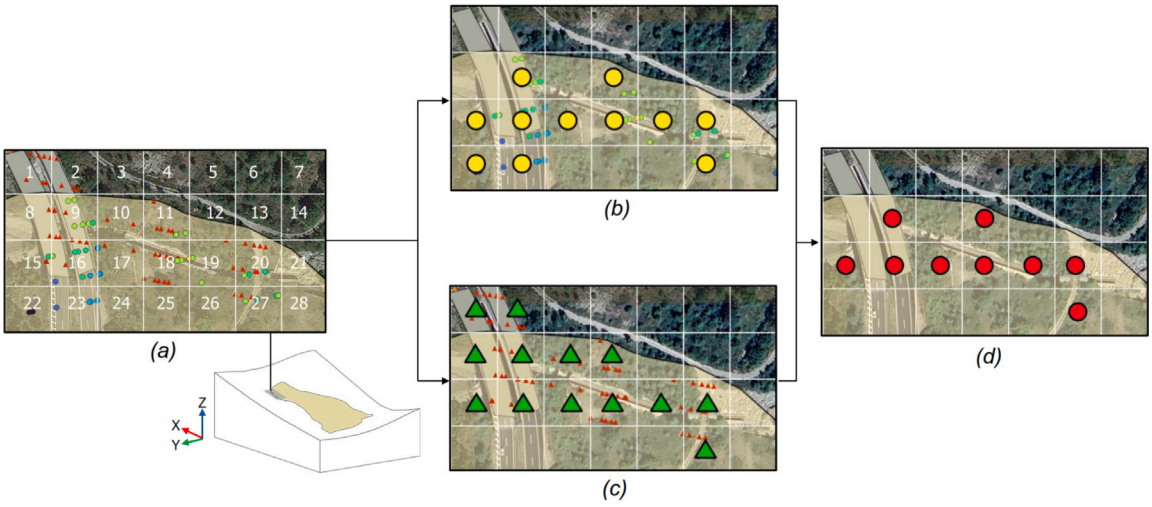

Fig. 7. Combination schema of ascending and descending datasets: (a) Resampling grid, (b) Ascending synthetic PS, (c) Descending synthetic PS, (d) Combined Synthetic PS.

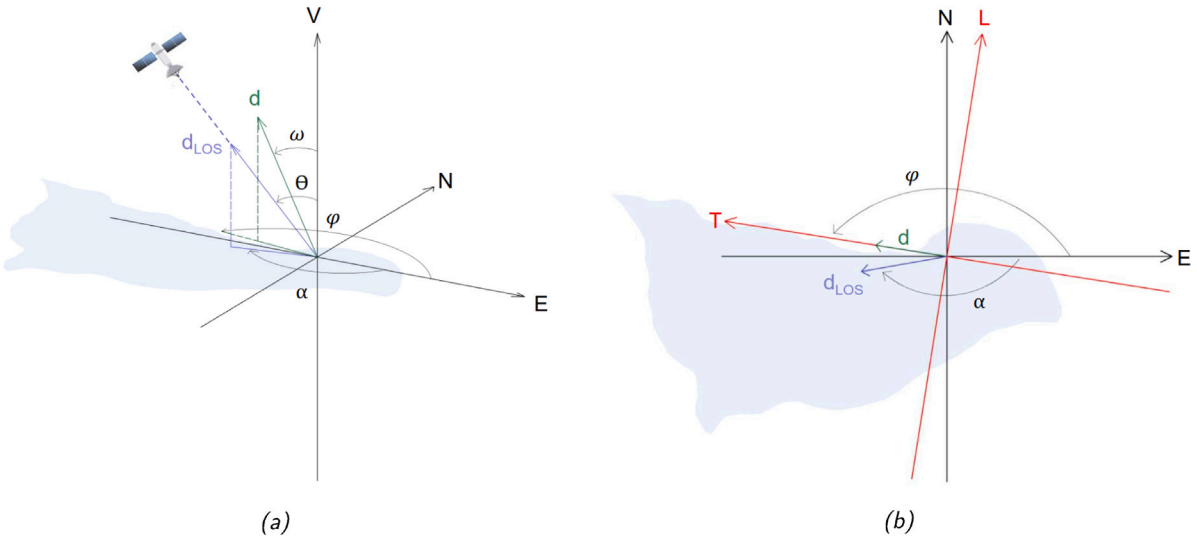

Fig. 8. Representation of: (a) global reference system (N, E, V); (b) local reference system fixed to the deformation phenomenon (L, T, V).

in the adopted local reference system (TLN), corresponds to the T-axis. Consequently, all displacements can be described as a two-dimensional deformation vector (d_T, d_V), making it possible to solve the system using only two observation geometries.

$$\hat{\mathbf{d}} = \mathbf{B}^{-1}\mathbf{d}_{LOS} \tag{7}$$

where:

$$\hat{\mathbf{d}} = \begin{Bmatrix} d_T \\ d_V \end{Bmatrix},$$

$$\mathbf{B} = \begin{bmatrix} \sin\theta_A \cos(\alpha_A + \varphi) & \cos\theta_A \\ \sin\theta_D \sin(\alpha_D + \varphi) & \cos\theta_D \end{bmatrix}$$

In this context, $\hat{d}$ represents the estimated components of the real displacement (d_T, d_V) and B is a sub-matrix of matrix A, obtained by removing the column associated with the component assumed to be zero (d_L). This formulation enables the conversion of the ascending (d_A) and descending (d_D) LOS measurements into the two main components of real displacement, providing an accurate two-dimensional description of the phenomenon.

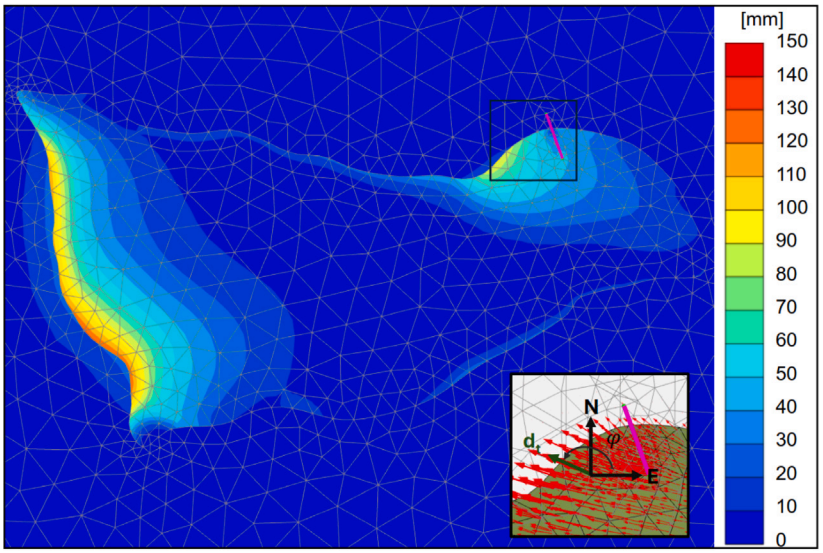

Fig. 9. Top view of the total displacement contours $|u|$ predicted for the analysed model. At the bottom right, the red arrows indicate the main direction of actual landslide movement within the NE plane.

Table 3
Horizontal displacements (u_x e u_y) recorded at the top and base of the piers and abutments.

Piers	u_x (mm)	u_y (mm)
Top Abutment 1	−4	9
Base Abutment 1	−2	4
Top Pier 1	−18	6
Base Pier 1	−11	3
Top Pier 2	−34	2.36
Base Pier 2	−35	5.25
Top Abutment 2	−35	2.35
Base Abutment 2	−36	5.82

4. Results

4.1. Analysis of the numerical simulation results

Numerical modelling allowed the analysis of both the response of the slope and the deformations induced on the bridge, providing a comprehensive view of the final equilibrium configuration of the system under stationary conditions. The numerical results reveal a non-uniform spatial distribution of total displacements ($|u|$) within the landslide volume (Fig. 9). In the downstream area, displacements reach their maximum values, approximately 14 cm, indicating greater movement magnitude in this portion of the landslide. Conversely, in the upstream area, displacements are more limited, around 10 cm, while near the bridge, values decrease further, stabilising at approximately 4 cm. This reduction reflects the mitigating effect exerted by the presence of the bridge on the displacement magnitude in the surrounding area. A detailed analysis of the displacement components reveals a predominant trend in the horizontal components u_x and u_y, which reach values of up to −3cm and 2.5 cm, respectively, while the vertical component is negligible. This behaviour is consistent with the kinematics of the landslide phenomenon, characterised by predominantly horizontal movements, confirming the observed sliding mechanism.

Regarding the response of the structural elements to the landslide movement, the analysis focused on the bridge piers and their foundation structures. Specifically, displacements were evaluated at the nodes located at the base of each pier, corresponding to the top of the foundation structure, and at the pier heads, in correspondence with the deck (Fig. 10a). The results presented in Table 3 and in Fig. 10b indicate that the elements located within the landslide-affected area (Pier 2 and Abutment 2) undergo significant displacements at their bases, aligned with the direction of the landslide movement. This suggests that the horizontal thrust exerted by the sliding volume primarily impacts the lower part of the structures, causing a downslope inclination. In contrast, Abutment 1, positioned outside the landslide volume, shows minimal displacements in the opposite direction, indicating negligible interaction with the landslide. Pier 1, situated in an intermediate zone, exhibits greater displacements than Abutment 1, reflecting a gradual increase in interaction with the landslide activity. These findings underline that piers located within or in close proximity to the landslide volume are substantially affected by the forces generated by the landslide movement.

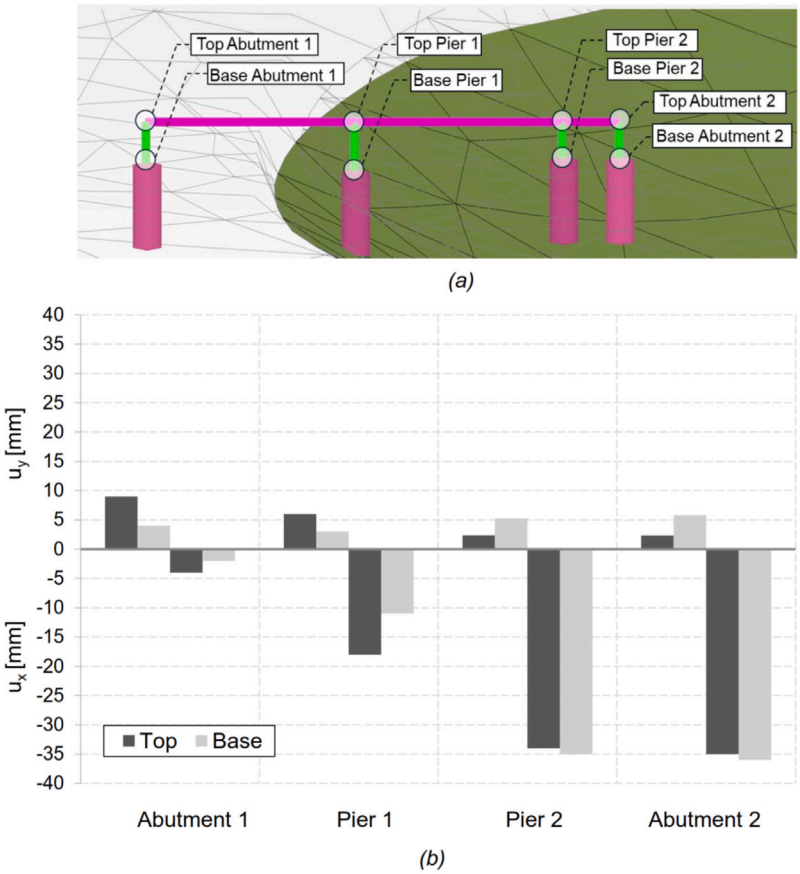

Fig. 10. (a) Selected control points for the analysed bridge; (b) Graphical representation of horizontal displacements (u_x e u_y) recorded at the top and base of the piers and abutments.

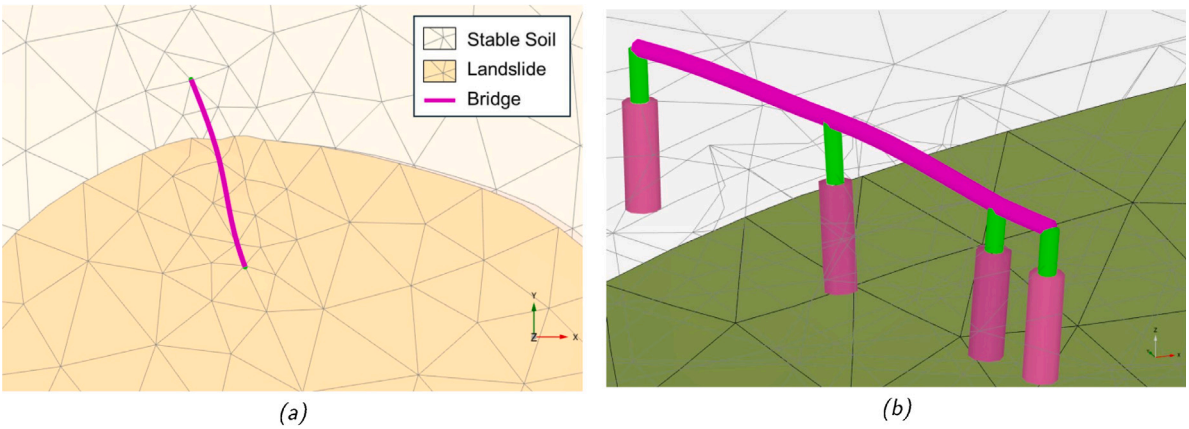

Fig. 11. Representation of: (a) Top view and (b) Perspective view of the bridge deformation mechanism.

To assess the overall stability of the integrated system comprising the bridge and the slope, a global safety factor analysis was performed. This analysis evaluated the system's capacity to maintain equilibrium under critical conditions, such as increased loads or substantial variations in strength parameters. The calculated value of 1.2274 indicates a condition close to the limit of stability, requiring continuous monitoring to mitigate potential risks. Furthermore, the deformation mechanism of the soil revealed by the analysis confirms the predictions based on the qualitative assessment, highlighting a rotational sliding of the landslide volume in the downstream direction. Furthermore, observing the deformation mechanism of the bridge from a top view (Fig. 11a and b), it

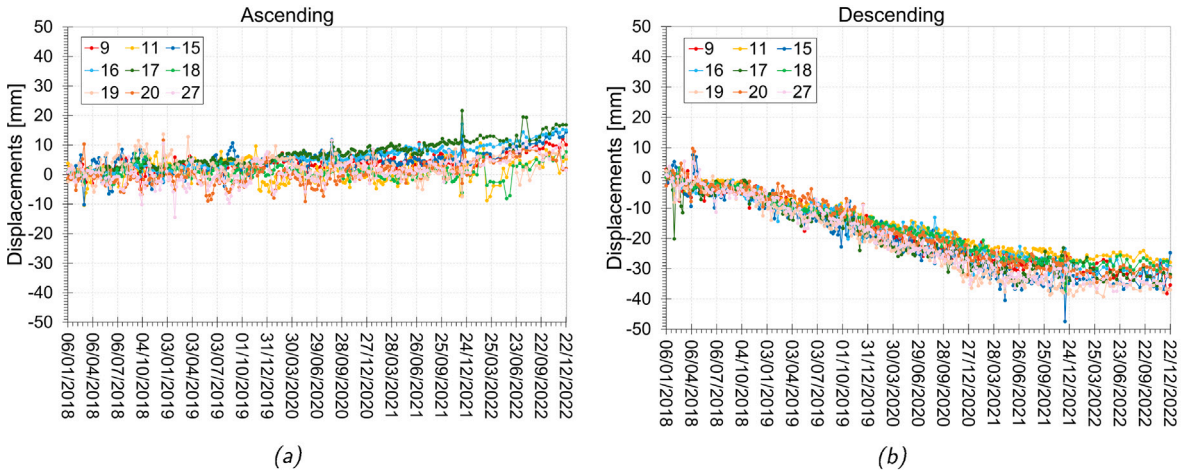

Fig. 12. Time evolution of displacements along the LOS in (a) ascending and (b) descending geometries for synthetic PS defined on a 25 m grid.

is evident that the infrastructure within the landslide area is dragged in the direction of the landslide movement. This dragging effect is primarily caused by the horizontal thrust exerted by the moving landslide volume, which acts on the bridge foundations, resulting in deformation consistent with the predominant direction of the landslide kinematics.

4.2. Analysis of satellite radar data

The post-processing procedure for displacement decomposition required combining PS data derived from ascending and descending orbital geometries. As described in Section 3, accurately estimating the components of actual displacement depends on acquisitions that are independent and coincident both spatially and temporally. To ensure these conditions, a resampling method based on a regular mesh with 25 m sides was adopted.

The results provided a single temporal evolution of displacements along the LOS for each synthetic PS, corresponding to the two orbits, as shown in Fig. 12. Analysis of the time distribution of LOS displacements in ascending and descending geometries reveals that the synthetic PS within the mobilised soil volume exhibit opposite-signed deformation measurements in the ascending and descending orbits. This behaviour is consistent with the kinematics under investigation, which is typical of landslides characterised by predominantly horizontal deformation components.

To confirm these observations, positive LOS values are recorded in the ascending geometry, which, by convention, indicate ground movement towards the satellite. Since the satellite observes westward in this configuration, this implies a horizontal movement component in that direction. Conversely, in the descending orbit, negative LOS values are observed, representing ground movement away from the satellite. Given that the satellite observes eastward in this configuration, the negative sign confirms the same horizontal movement direction towards the west. This consistency between the two geometries highlights a coherent westward movement of the landslide. Furthermore, the combined analysis revealed a predominant horizontal component, aligning with the expected behaviour of the analysed landslide.

Once the PS data from the two observation geometries, ascending and descending, were combined, it became possible to estimate the three-dimensional displacement field. The approach used to estimate the components of actual displacement, described in Section 3, involves adopting a local reference system oriented along the real displacement direction of the landslide in the horizontal plane, determined by numerical modelling. Assuming that displacements in the longitudinal direction are negligible, the values of the real displacement vector components along the transverse and vertical directions were estimated for the synthetic PS within the area of interest. The results revealed a generally stable behaviour over time for the synthetic PS located within the meshes of the landslide area. The transverse component (d_T) shows a progressive increase, reaching values of approximately 40 mm towards the end of the monitoring period (Fig. 13a), while the vertical component (d_V) records a progressive lowering of up to approximately −20 mm during the same period (Fig. 13b). These findings clearly reflect the dynamics of the analysed landslide, which predominantly develops along the horizontal plane, with a less significant but non-negligible vertical component.

5. Discussion

The analysis of InSAR data required a comparative assessment of different resampling methods to identify the most suitable configuration for ensuring a homogeneous and reliable representation of displacements. The method proposed by Notti et al. [20], based on pairing a PS from one geometry with the closest PS from the other geometry within a buffer-defined distance (Fig. 14a), involves linear interpolation to temporally align the datasets by estimating the missing displacement values on non-common dates. Although this method yielded a greater number of synthetic points compared to the approach adopted in this study, the resulting

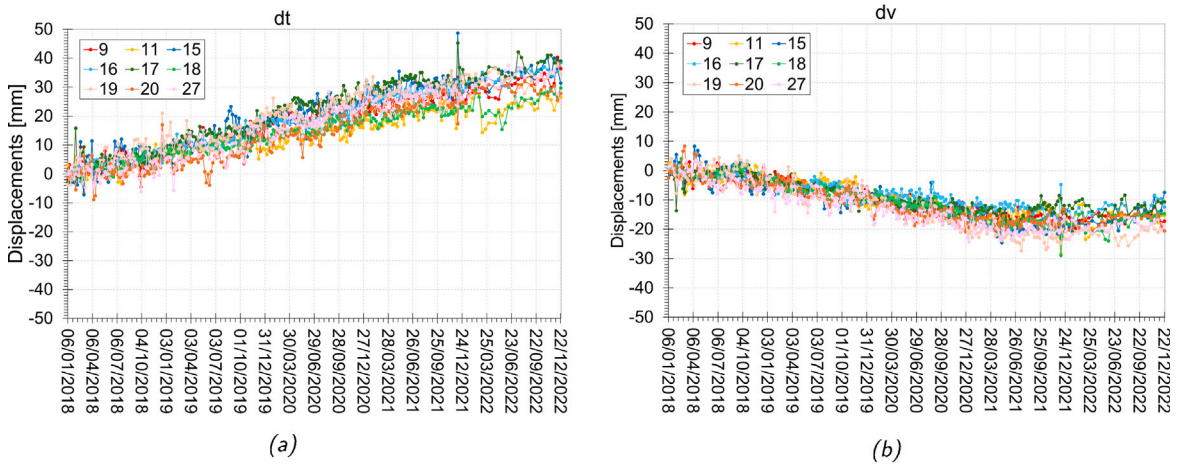

Fig. 13. Time evolution of the two components of the actual displacement of the identified synthetic PS: (a) transverse (d_T) and (b) vertical (d_V).

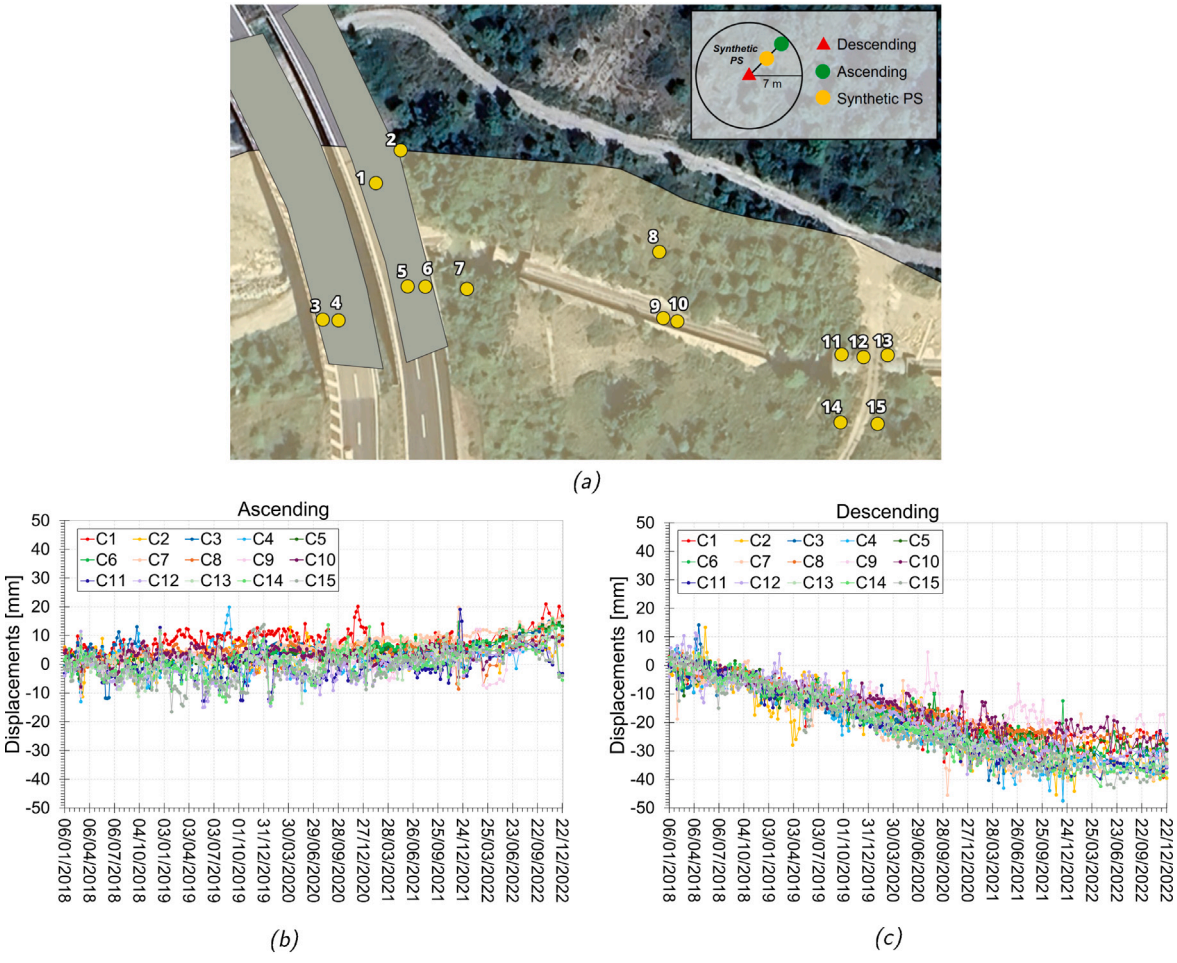

Fig. 14. (a) Determination of synthetic PS using a defined buffer distance and (b-c) time evolution of displacements along the LOS in ascending (b) and (c) descending geometries for synthetic PS defined on a buffer distance.

trends exhibited significant outliers (Fig. 14b), with values deviating considerably from the rest of the dataset. These outliers can be attributed to the presence of vegetation, whose signal is affected by wind influence and seasonal variations.

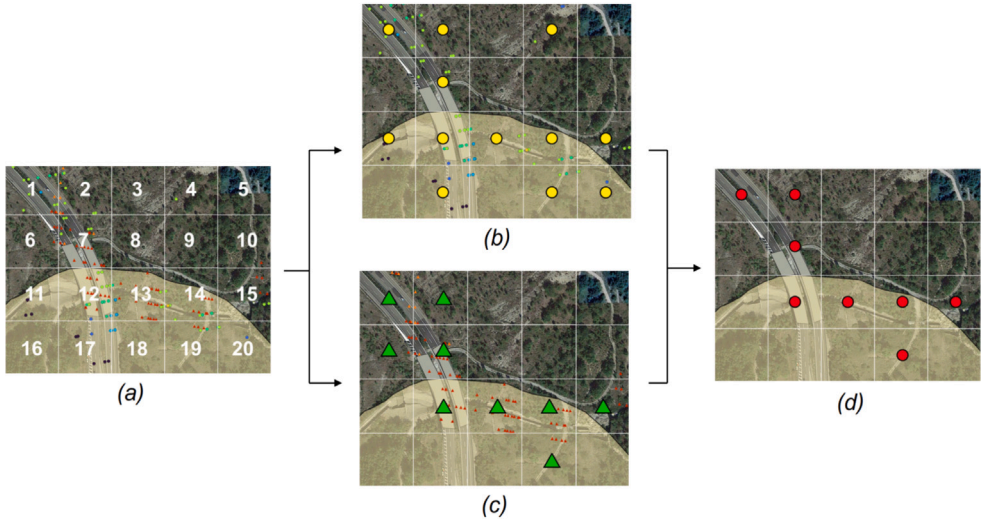

Fig. 15. Combination schema of ascending and descending datasets, with 50 m side grid: (a) Resampling grid, (b) Ascending synthetic PS, (c) Descending synthetic PS, (d) Combined Synthetic PS.

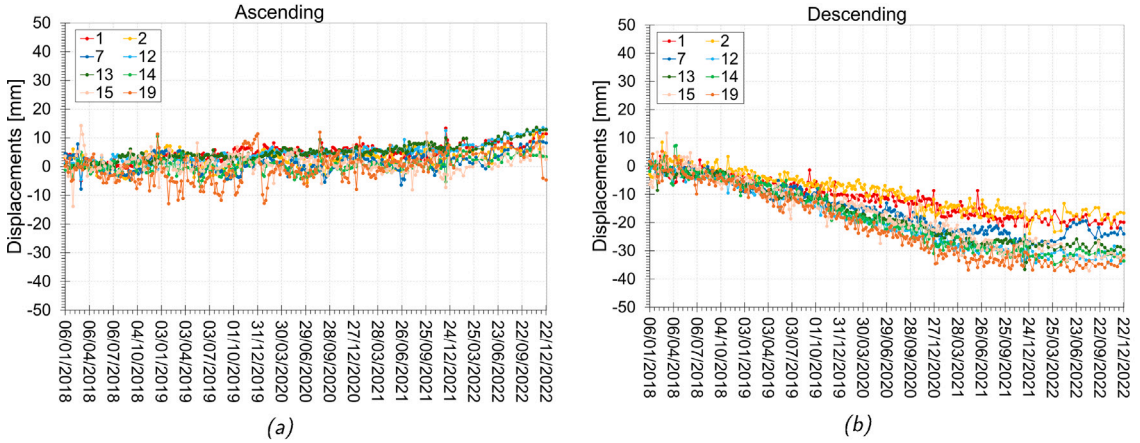

Fig. 16. Time evolution of displacements along the LOS in (a) ascending and (b) descending geometries for synthetic PS defined on a 50 m grid.

To mitigate these effects, the regular grid method proposed by Casagli et al. [26], described in detail in Section 3, was considered. This approach, based on averaging displacements within cells with a side length of 50 m (Fig. 15), reduced the presence of outliers, improving data stability. However, using a grid of this size resulted in a loss of detail in the description of the landslide kinematics (Fig. 16), limiting the ability to detect local variations in movement. For this reason, a grid with a side length of 25 m was adopted as an effective compromise, ensuring a more homogeneous data distribution and reducing the influence of outliers by averaging points with more similar behaviour.

Once the optimal resampling configuration was defined and the displacements of the synthetic PS were estimated, it was possible to compare the results with instrumental monitoring measurements. Although the spatial coverage of traditional monitoring is broader, encompassing both the upper and lower portions of the landslide, whereas InSAR data are primarily concentrated in the upper part, the comparison was carried out using the topographic targets closest to the identified synthetic PS, namely targets 2, 5, 7, and 8 (Fig. 17). Their proximity allowed for a more consistent assessment of displacement evolution compared to other measurement points. Considering these targets, between 1975 and 1999, the recorded average movement was approximately 1.05 m, with a velocity of 4 cm/year, while between 2004 and 2015, the movement decreased to 0.26 m over 11 years, corresponding to an average velocity of 2 cm/year (Fig. 3c). InSAR data for the period 2018–2022 confirm this trend, indicating a further slowdown, with a maximum displacement of 40 mm (Fig. 13), equivalent to an average velocity of 1 cm/year. This progressive trend is consistent with the long-term behaviour of the landslide and may reflect its natural evolution under relatively stable external conditions.

In addition to the comparison with instrumental monitoring, a qualitative assessment was conducted between the displacements derived from the InSAR analysis and the results of numerical modelling. Given the different nature of the two approaches, a

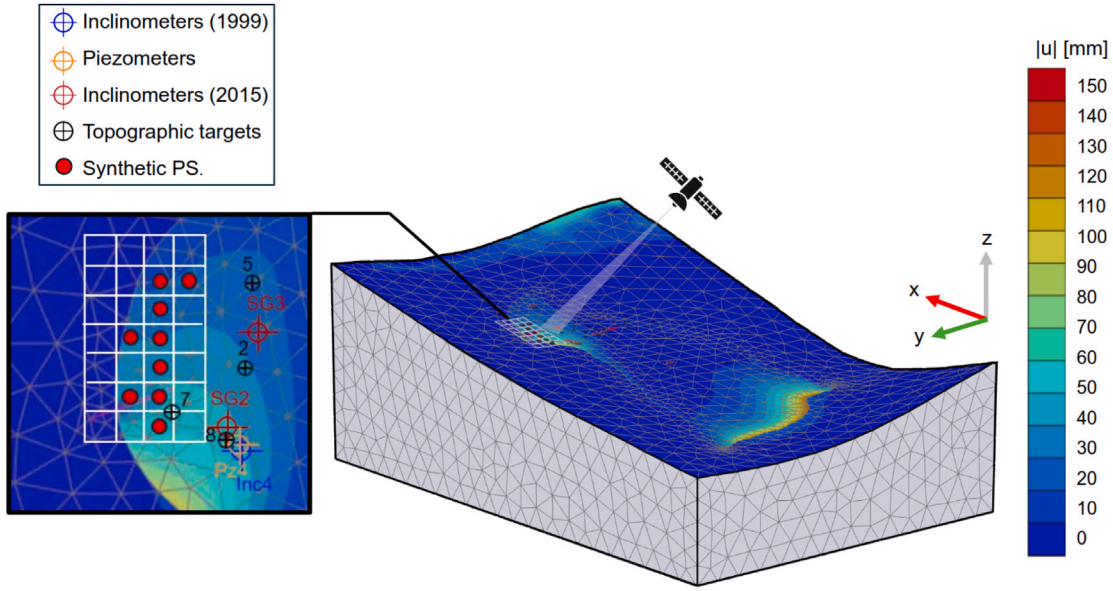

Fig. 17. Total displacements from numerical modelling (Fig. 9) with overlaid instrumental monitoring data (Fig. 3a) and synthetic PS (Fig. 7d) identified using the 25 m grid resampling method.

direct quantitative comparison is not feasible: interferometric data describe the transient evolution of the phenomenon during the observation period, whereas numerical modelling provides a final steady-state configuration of the landslide, simulating deformations under the limit equilibrium condition. However, the qualitative comparison revealed a good correlation in the spatial distribution of the areas experiencing the highest movement (Fig. 17). Specifically, in the upper portion of the landslide, InSAR data confirmed the critical areas identified by numerical modelling. In the lower portion, on the other hand, the absence of satellite data prevented a direct comparison, but numerical modelling indicated significant displacements, suggesting a higher intensity of movement in this area.

6. Conclusions

The integrated approach proposed in this study, which combines InSAR satellite interferometry with three-dimensional numerical modelling of landslides interacting with bridges, has proven highly effective in a significant case study. The proposed methodology highlights how the integration of satellite monitoring techniques and numerical models provides complementary and more detailed information compared to the isolated use of each approach. In particular, the InSAR analysis provided a global view of surface deformations, but the one-dimensional nature of the measurements along the sensor's Line of Sight (LOS) limits the ability to describe the phenomenon in three-dimensional terms. In this context, numerical modelling proves to be a valuable complementary tool that overcomes this limitation, aiding in the reconstruction of actual displacement components and accurately identifying the primary direction of landslide movement. The results from the satellite analysis highlighted predominant transverse movements and a less significant vertical component, consistent with the observed kinematics. Furthermore, InSAR data, with its capacity to cover large areas and monitor deformations over time, expanded the information provided by traditional monitoring methods. Although the latter played a crucial role in calibrating the numerical model and providing precise local measurements, the combined use of InSAR enabled a broader and more detailed understanding of the landslide phenomenon, facilitating the comprehension of its behaviour at a regional scale. The results of the numerical modelling provided a detailed representation of the interactions between the landslide phenomenon and the bridge, highlighting a spatially variable distribution of displacements. In particular, greater movement intensity was observed in the downstream portion of the landslide, decreasing further near the bridge, reflecting the role of the infrastructure in mitigating the intensity of displacements in its surrounding area. The qualitative comparison between the two methodologies, despite their differences — one being stationary and the other based on continuous monitoring over a four-year period — proved essential for assessing the consistency between the numerical simulations and the observed data. In particular, a good match was observed in the areas upstream of the landslide, where the satellite data confirmed the critical areas identified by the numerical modelling, showing good agreement with the displacements recorded by traditional monitoring. In contrast, downstream, the lack of satellite data prevented a direct comparison. However, the missing information was filled by the numerical modelling, which highlighted significant displacements, indicating a higher intensity of movement in this portion of the landslide. In conclusion, the combination of these two methodologies has provided a more comprehensive and accurate understanding of the landslide phenomenon. By integrating large-scale surface displacement monitoring with a detailed mechanical characterisation of the landslide, this approach improves the interpretation of ground deformations and the estimation of displacement components.

These results contribute to a more accurate assessment of landslide-induced effects on infrastructure stability, offering valuable insights for the identification of critical areas and supporting informed decision-making in the context of long-term monitoring and mitigation strategies.

CRediT authorship contribution statement

Erica Cernuto: Writing – original draft, Visualization, Methodology, Investigation, Conceptualization. **Diana Salciarini:** Writing – review & editing, Supervision, Methodology, Investigation, Conceptualization. **Filippo Ubertini:** Writing – review & editing, Supervision, Conceptualization. **Giorgia Giardina:** Writing – review & editing, Supervision, Methodology, Investigation, Conceptualization.

Funding

Authors acknowledge funding from FABRE Consortium within the activities of the FABRE-ANAS 2021–2024 research program. This publication is also part of the Vidi project InStruct, project number 18912, financed by the Dutch Research Council (NWO).

Declaration of competing interest

The authors declare that they have no known competing financial interests or personal relationships that could have appeared to influence the work reported in this paper.

Acknowledgements

This study was supported by FABRE – "Research consortium for the evaluation and monitoring of bridges, viaducts and other structures" (www.consorziofabre.it/en) within the activities of the FABRE-ANAS and FABRE-ASTM 2021–2026 research programs. Any opinion expressed in the paper does not necessarily reflect the view of the funder. Additionally, this research was supported by the project "Methodological Approaches for RIsk assessment in the framework of landslide bridge IntEraction (MARIE)". The authors would also like to thank ASTM for sharing the data used in this study; the views expressed in the paper are those of the authors and do not necessarily represent those of ASTM.

Data availability

Data will be made available on request.

References

[1] F. Ponziani, N. Berni, M. Stelluti, R. Zauri, C. Pandolfo, L. Brocca, T. Moramarco, D. Salciarini, C. Tamagnini, LANDWARN: an operative early warning system for landslides forecasting based on rainfall thresholds and soil moisture, in: Landslide Science and Practice: Volume 2: Early Warning, Instrumentation and Monitoring, Springer, 2013, pp. 627–634.
[2] D. Salciarini, E. Volpe, S.A. Kelley, L. Brocca, S. Camici, G. Fanelli, C. Tamagnini, Modeling the effects induced by the expected climatic trends on landslide activity at large scale, Procedia Eng. 158 (2016) 541–545.
[3] D.A. Salcedo, Behavior of a landslide prior to inducing a viaduct failure, Caracas–La Guaira highway, Venezuela, Eng. Geol. 109 (1–2) (2009) 16–30.
[4] G. Luo, X. Hu, E. Bowman, J. Liang, Stability evaluation and prediction of the Dongla reactivated ancient landslide as well as emergency mitigation for the Dongla Bridge, Landslides 14 (2017) 1403–1418.
[5] S. He, S. Yan, Y. Deng, W. Liu, Impact protection of bridge piers against rockfall, Bull. Eng. Geol. Environ. 78 (2019) 2671–2680.
[6] F. Gabrieli, F. Gibin, L. Brezzi, E. Cernuto, A. Lupatelli, D. Salciarini, E. Mammoliti, F. Dezi, S. Stacul, N. Squeglia, et al., Lessons from international case studies on bridge-slide interaction problems, Procedia Struct. Integr. 62 (2024) 506–513.
[7] D. Salciarini, E. Cernuto, G. Capati, F. Dezi, L. Brezzi, F. Gibin, F. Gabrieli, S. Stacul, A. Doglioni, A. Lupattelli, et al., Landslide-bridge interaction: Insights from an extensive database of Italian case studies, Int. J. Disaster Risk Reduct. 114 (2024) 104983.
[8] M. Barla, S. Aiassa, F. Antolini, V. Vezzaro, On the interaction between a large landslide and a bridge, Procedia Struct. Integr. 62 (2024) 585–592.
[9] M. Loli, A. Chatzidaki, D. Vamvatsikos, G. Gazetas, K. Bakalis, E. Hernández-Montes, L.M. Gil-Martín, Seismic vulnerability of motorway bridge on active landslide, in: 17th World Conference on Earthquake Engineering, 17WCEE, 2020, pp. 1–12.
[10] F. Bellotti, M. Bianchi, D. Colombo, A. Ferretti, A. Tamburini, Advanced InSAR techniques to support landslide monitoring, in: Mathematics of Planet Earth: Proceedings of the 15th Annual Conference of the International Association for Mathematical Geosciences, Springer, 2013, pp. 287–290.
[11] L. Solari, M. Del Soldato, F. Raspini, A. Barra, S. Bianchini, P. Confuorto, N. Casagli, M. Crosetto, Review of satellite interferometry for landslide detection in Italy, Remote. Sens. 12 (8) (2020) 1351.
[12] S. Moretto, F. Bozzano, P. Mazzanti, The role of satellite InSAR for landslide forecasting: Limitations and openings, Remote. Sens. 13 (18) (2021) 3735.
[13] E. Ghaderpour, C. Masciulli, M. Zocchi, F. Bozzano, G. Scarascia Mugnozza, P. Mazzanti, Estimating reactivation times and velocities of slow-moving landslides via PS-InSAR and their relationship with precipitation in central Italy, Remote. Sens. 16 (16) (2024) 3055.
[14] N. Casagli, F. Catani, G. Falorni, P. Lu, et al., Landslide monitoring through satellite and ground-based radar interferometry, in: Proceedings of the 10th International Symposium on Landslides and Engineered Slopes, CRC Press, 2008, pp. 1–6.
[15] A. Ferretti, A. Monti-Guarnieri, C. Prati, F. Rocca, D. Massonet, InSAR Principles-Guidelines for SAR Interferometry Processing and Interpretation, vol. 19, 2007.
[16] V. Macchiarulo, P. Milillo, C. Blenkinsopp, C. Reale, G. Giardina, Multi-temporal InSAR for transport infrastructure monitoring: recent trends and challenges, in: Proceedings of the Institution of Civil Engineers-Bridge Engineering, vol. 176, no. 2, Thomas Telford Ltd, 2021, pp. 92–117.

[17] J. Hu, Z. Li, X. Ding, J. Zhu, L. Zhang, Q. Sun, Resolving three-dimensional surface displacements from InSAR measurements: A review, Earth-Sci. Rev. 133 (2014) 1–17.
[18] X. Liu, C. Zhao, Q. Zhang, Y. Yin, Z. Lu, S. Samsonov, C. Yang, M. Wang, R. Tomás, Three-dimensional and long-term landslide displacement estimation by fusing C-and L-band SAR observations: A case study in Gongjue County, Tibet, China, Remote Sens. Environ. 267 (2021) 112745.
[19] C. Song, C. Yu, Z. Li, V. Pazzi, M. Del Soldato, A. Cruz, S. Utili, Landslide geometry and activity in villa de la independencia (Bolivia) revealed by InSAR and seismic noise measurements, Landslides 18 (8) (2021) 2721–2737.
[20] D. Notti, G. Herrera, S. Bianchini, C. Meisina, J.C. García-Davalillo, F. Zucca, A methodology for improving landslide PSI data analysis, Int. J. Remote Sens. 35 (6) (2014) 2186–2214.
[21] W. Brouwer, An Analysis of the Insar Displacement Vector Decomposition: Insar Fallacies and the Strap-Down Solution (Master's thesis), Delft University of Technology, 2021.
[22] C. Proietti, Interpretazione di dati radar satellitari per la valutazione di movimenti di massa localizzati (Ph.D. thesis), Dipartimento Scienza della terra, Università degli studi di Firenze, 2009.
[23] E. Farneti, N. Cavalagli, M. Costantini, F. Trillo, F. Minati, I. Venanzi, F. Ubertini, A method for structural monitoring of multispan bridges using satellite InSAR data with uncertainty quantification and its pre-collapse application to the Albiano-Magra Bridge in Italy, Struct. Heal. Monit. 22 (1) (2023) 353–371.
[24] E. Farneti, N. Cavalagli, I. Venanzi, W. Salvatore, F. Ubertini, Residual service life prediction for bridges undergoing slow landslide-induced movements combining satellite radar interferometry and numerical collapse simulation, Eng. Struct. 293 (2023) 116628.
[25] M. Manzo, G. Ricciardi, F. Casu, G. Ventura, G. Zeni, S. Borgström, P. Berardino, C. Del Gaudio, R. Lanari, Surface deformation analysis in the Ischia Island (Italy) based on spaceborne radar interferometry, J. Volcanol. Geotherm. Res. 151 (4) (2006) 399–416.
[26] N. Casagli, C. Proietti, G. Righini, F. Cigna, V. Pancioli, A. Colombo, F. Poggi, P. Cantone, F. Galluccio, D. Colombo, et al., Piano Straordinario di Telerilevamento Ambientale: Linee guida per l'analisi dei dati interferometrici satellitari in aree soggette a dissesti idrogeologici, Ministero dell'Ambiente e della Tutela del Territorio e del Mare, Italy, 2009, Technical guidelines.
[27] T. Styles, D. Stead, E. Eberhardt, B. Rabus, M. Gaida, J. Bloom, Integrated numerical modelling and insar monitoring of a slow moving slope instability at bingham canyon mine, Proc. Slope Stab. (2011).
[28] P. Ma, Y. Cui, W. Wang, H. Lin, Y. Zhang, Coupling InSAR and numerical modeling for characterizing landslide movements under complex loads in urbanized hillslopes, Landslides 18 (2021) 1611–1623.
[29] D. Sun, W. Deng, T. Yang, J. Li, Y. Zhao, A case study integrating numerical simulation and InSAR monitoring to analyze bedding-controlled landslide in nanfen open-pit mine, Sustainability 15 (14) (2023) 11158.
[30] A. Meoni, L. Ierimonti, E. Farneti, M. Castellani, F. Filippucci, A. Natali, S. Celati, F. Scozzese, M. Morici, N. Cavalagli, et al., A new methodology for the diagnosis and monitoring of bridges under slow deformation phenomena, Int. J. Bridg. Eng. Manag. Res. 1 (1) (2024) 1–13.
[31] A. Morcioni, T. Apuani, F. Cecinato, Piuro landslide: 3D hydromechanical numerical modelling of the 1618 event, Geosciences 13 (2) (2023) 49.
[32] G. Bru, J.A. Fernández-Merodo, J. García-Davalillo, G. Herrera, J. Fernández, Site scale modeling of slow-moving landslides, a 3D viscoplastic finite element modeling approach, Landslides 15 (2018) 257–272.
[33] B. François, L. Tacher, C. Bonnard, L. Laloui, V. Triguero, Numerical modelling of the hydrogeological and geomechanical behaviour of a large slope movement: the Triesenberg landslide (Liechtenstein), Can. Geotech. J. 44 (7) (2007) 840–857.
[34] Y.x. Hu, Z.y. Yu, J.w. Zhou, Numerical simulation of landslide-generated waves during the 11 October 2018 Baige landslide at the Jinsha River, Landslides 17 (10) (2020) 2317–2328.
[35] D. Salciarini, A. Lupattelli, F. Cecinato, E. Cattoni, E. Volpe, et al., Static and seismic numerical analysis of a shallow landslide located in a vulnerable area, RIG (2022) 2–2.
[36] Q. Xie, Z. Cao, R. Tian, W. Sun, A. Fumagalli, H. Peng, X. Fu, H. Luo, Complex sliding characteristics of landslides and evaluation of the reinforcement with arched anti-slide piles based on 3D discrete element method: a case study, Nat. Hazards (2024) 1–25.
[37] H. Gardezi, M. Bilal, Q. Cheng, A. Xing, Y. Zhuang, T. Masood, A comparative analysis of attabad landslide on January 4, 2010, using two numerical models, Nat. Hazards 107 (2021) 519–538.
[38] J. Wei, Z. Zhao, C. Xu, Q. Wen, Numerical investigation of landslide kinetics for the recent Mabian landslide (Sichuan, China), Landslides 16 (2019) 2287–2298.
[39] M. Breccolotti, A.L. Materazzi, D. Salciarini, C. Tamagnini, F. Ubertini, et al., Vibrations induced by the new underground railway line in Palermo, Italy experimental measurements and FE modeling, in: Proceedings of the 8th International Conference on Structural Dynamics, Leuven, Belgium, 2011, pp. 719–726.
[40] G. Pappalardo, D. Caliò, L. Cavallaro, A. Musca, D. Rapicavoli, F. Cannizzaro, I. Caliò, Multi-hazard assessment of a masonry railway bridge in landslide areas, Procedia Struct. Integr. 62 (2024) 460–467.
[41] A. Mantakas, A. Tsatsis, M. Loli, R. Kourkoulis, G. Gazetas, Seismic response of a motorway bridge founded in an active landslide: a case study, Bull. Earthq. Eng. 21 (1) (2023) 605–632.
[42] E. Pilecka, D. Szwarkowski, J. Stanisz, M. Blockus, Analysis of a landslide on a railway track using laser scanning and FEM numerical modelling, Appl. Sci. 12 (15) (2022) 7574.
[43] R. Bovolenta, D. Bianchi, Geotechnical analysis and 3D fem modeling of Ville San Pietro (Italy), Geosciences 10 (11) (2020) 473.
[44] F. Cotecchia, F. Santaloia, V. Tagarelli, Towards a geo-hydro-mechanical characterization of landslide classes: Preliminary results, Appl. Sci. 10 (22) (2020) 7960.
[45] D. Salciarini, D. Pauselli, E. Cernuto, G. Boco, F. Ubertini, Analysis of the interaction of a landslide with viaduct foundations under static and dynamic conditions, Procedia Struct. Integr. 62 (2024) 514–521.
[46] K.J. Reinders, G. Giardina, F. Zurfluh, J. Ryser, R.F. Hanssen, Proving compliance of satellite InSAR technology with geotechnical design codes, Transp. Geotech. 33 (2022) 100722.
[47] A. Innocenti, A. Rosi, V. Tofani, V. Pazzi, E. Gargini, E.B. Masi, S. Segoni, D. Bertolo, M. Paganone, N. Casagli, Geophysical surveys for geotechnical model reconstruction and slope stability modelling, Remote. Sens. 15 (8) (2023) 2159.
[48] V. Tofani, F. Raspini, F. Catani, N. Casagli, Persistent Scatterer Interferometry (PSI) technique for landslide characterization and monitoring, Remote. Sens. 5 (3) (2013) 1045–1065.
[49] Idrogeo, Inventory of landlside phenomena in Italy, https://idrogeo.isprambiente.it/.
[50] Regione Emilia-Romagna, Servizi moka - GeoApp, 2025, cartageologica. URL: https://servizimoka.regione.emilia-romagna.it/mokaApp/apps/geo/index.html.
[51] R. Brinkgreve, S. Kumarswamy, W. Swolfs, D. Waterman, A. Chesaru, P. Bonnier, et al., PLAXIS 2016, 2016, pp. 1–16, PLAXIS Bv, the Netherlands.
[52] N.B. Salih, T.A. Abdalla, F.A. Ahmed, Soil-foundation interaction and its influences on some geotechnical properties of sulaimaniyah, northern Iraq fine-grained soils utilizing plaxis 3D, Eng. Technol. J. 41 (5) (2023) 642–651.
[53] D. Salciarini, D. Pauselli, G. Temperoni, Effects of complex surface conditions on the seismic response of caisson foundations, in: Geotechnical Engineering in the Digital and Technological Innovation Era, Springer, 2023, pp. 687–695.
[54] B.D. Teji, A.A. Ashango, Performance optimization of piled raft foundations in layered soil under uniform vertical loading using plaxis 3D, Adv. Mater. Sci. Eng. 2023 (1) (2023) 6693876.

[55] D. Pauselli, D. Salciarini, F. Ubertini, Three-dimensional modeling of soil-structure interaction for a bridge founded on caissons under seismic conditions, Appl. Sci. 12 (21) (2022) 10904.
[56] R. Emilia-Romagna, Cartografia della Regione Emilia-Romagna, https://mappe.regione.emilia-romagna.it/.
[57] K. Terzaghi, R.B. Peck, G. Mesri, Soil Mechanics in Engineering Practice, John Wiley & Sons, 1996.
[58] T. Schanz, Modellierung des mechanischen verhaltens von reibungsmaterialien, habilitations schrift, mitteilung 45 des instituts fur geotechnik, Universit at Stuttgart, 1998.
[59] T. Schanz, P. Vermeer, P.G. Bonnier, The hardening soil model: Formulation and verification, in: Beyond 2000 in Computational Geotechnics, Routledge, 2019, pp. 281–296.
[60] T. Schanz, P. Vermeer, P. Bonnier, Formulation and verification of the hardening-soil model, in: Beyond 2000 in Computational Geotechnics, 1999, pp. 1–16.
[61] B. Systems, Material models manual, 2020, connect edition v20.04 ed., Bentley Systems, PLAXIS Software Documentation.
[62] N. Janbu, Soil compressibility as determined by oedometer and triaxial tests, in: Proc. European Conf. SMFE, Wiesbaden, 1963, vol. 1, 1963, pp. 19–25.
[63] J.T. Wu, S.C.Y. Tung, Determination of model parameters for the hardening soil model, Transp. Infrastruct. Geotechnol. 7 (1) (2020) 55–68.
[64] EA, European ground motion service (EGMS), https://egms.land.copernicus.eu, Copernicus.
[65] M. Costantini, F. Minati, F. Trillo, A. Ferretti, F. Novali, E. Passera, J. Dehls, Y. Larsen, P. Marinkovic, M. Eineder, et al., European ground motion service (EGMS), in: 2021 IEEE International Geoscience and Remote Sensing Symposium, IGARSS, IEEE, 2021, pp. 3293–3296.
[66] W.S. Brouwer, R.F. Hanssen, A treatise on InSAR geometry and 3D displacement estimation, IEEE Trans. Geosci. Remote Sens. (2023).